

**SYNERGETIC RADIOSENSITIZATION
EFFECTS OF BISMUTH OXIDE
NANOPARTICLES, CISPLATIN AND
BAICALEIN-RICH FRACTION FROM *Oroxylum*
indicum COMBINATIONS FOR CLINICAL
RADIOTHERAPY**

NOOR NABILAH BINTI TALIK SISIN

UNIVERSITI SAINS MALAYSIA

2021

**SYNERGETIC RADIOSENSITIZATION
EFFECTS OF BISMUTH OXIDE
NANOPARTICLES, CISPLATIN AND
BAICALEIN-RICH FRACTION FROM *Oroxylum*
indicum COMBINATIONS FOR CLINICAL
RADIOTHERAPY**

by

NOOR NABILAH BINTI TALIK SISIN

Thesis submitted in fulfillment of the requirements

for the degree of

Doctor of Philosophy

JUNE 2021

ACKNOWLEDGEMENT

Bismillahirrahmanirrahim.

Alhamdulillah for His endless blessings and strengths.

This thesis is dedicated to my supportive ***Ummi Hajjah Azimah, Ayah Haji Talib*** and my whole beloved family.

Deepest gratefulness to my inspiring supervisor and co-supervisors: **Dr. Wan Nordiana Wan Abd Rahman**, Prof. Dr. Khairunisak Abdul Razak and Dr. Nor Fazila Che Mat.

This work was also supported by Universiti Sains Malaysia Research University Grant (**RUI: 1001/PPSK/8012212**), using the special facilities from the Nuclear Medicine, Radiotherapy and Oncology Department, Hospital USM, the Central Research Laboratory, School of Medical Sciences, USM, and the International Institute for Halal Research and Training, IIUM.

Appreciations to the helpful Hospital USM staffs (Kak Tie and En. Reduan) and PPSK's postgraduate friends.

Lastly, special thankfulness to my awesome research groupmates: Kak Jo, Kak Mizah, Emi, Afiq, Nashrul, En. Safri and Amirah.

TABLE OF CONTENT

	Page
ACKNOWLEDGEMENT	ii
TABLE OF CONTENT	iii
LIST OF TABLES	x
LIST OF FIGURES	xii
LIST OF ACRONYMS, ABBREVIATIONS AND SYMBOLS.....	xix
ABSTRAK	xxvi
ABSTRACT	xxix
CHAPTER 1 INTRODUCTION	1
1.1 Introduction to Radiotherapy	1
1.2 Radiosensitization Mechanisms	3
1.2.1 Physical Phase	3
1.2.2 Chemical Phase	5
1.2.3 Biological Phase	7
1.3 Nanotechnology and Nanomedicine	8
1.4 Natural Compounds for Anti-Cancer Treatment	11
1.5 Problem Statement and Rationale of the Study	13
1.6 Objectives of the Study	17
1.7 Thesis Outline	18
1.8 Research Scopes	19
CHAPTER 2 LITERATURE REVIEW	21
2.1 Overview on Breast Cancers	21
2.2 The R's of Radiobiological Principles.....	25
2.2.1 The First Four Rs.....	25

2.2.2	The Fifth R: Radiosensitivity (Intrinsic)	28
2.2.3	Additional 6 th of the Rs	30
2.3	Cell Survival Curves Fitted to Linear-Quadratic (LQ) Model	31
2.4	Radiosensitizers in Radiotherapy	33
2.4.1	Application of High-Z Metallic Nanoparticles as Radiosensitizers	34
2.4.2	Application of Anti-cancer Drugs	39
2.4.3	Application of Natural Compounds.....	47
2.5	Molecular Characterization of Radiosensitization Effects	53
2.5.1	Reactive Oxygen Species (ROS).....	53
2.5.2	Apoptosis.....	57
2.5.3	Biochemical Changes Analysis by Raman Spectroscopy (RS).60	
CHAPTER 3 MATERIALS AND METHODS.....		64
3.1	Materials Used in the Study.....	64
3.1.1	Reagents and Materials.....	64
3.1.2	Equipments	65
3.1.3	Software.....	66
3.2	Methodology of the Study	66
3.3	Preparation of Treatment Components.....	67
3.3.1	Preparation of Bismuth Oxide Nanoparticles (BiONPs).....	67
3.3.2	Preparation of Cisplatin (Cis).....	70
3.3.3	Preparation of Baicalein-Rich Fraction (BRF).....	71
3.4	Cell Culture Protocols.....	72
3.5	Cytotoxicity Tests using PrestoBlue assay	74
3.5.1	Cytotoxicity of BiONPs	74

3.5.2	Cytotoxicity of Cis	76
3.5.3	Cytotoxicity of BRF	77
3.6	Reactive Oxygen Species (ROS) Measurement against BiONPs.....	78
3.7	Cellular Uptake and Localization of BiONPs in Cells	79
3.7.1	BiONPs Intracellular Localization Observation by Microscopy	79
3.7.2	BiONPs Cellular Uptake by Flow Cytometry	80
3.8	Cell Samples Irradiation Set Up	82
3.8.1	Treatment Components	82
3.8.2	High Dose Rate (HDR) Brachytherapy (^{192}Ir of γ -radiation)....	83
3.8.3	Megavoltage Photon Beam Therapy	84
3.8.4	Megavoltage Electron Beam Therapy	85
3.9	Post-irradiation Clonogenic Assay	86
3.10	Cell Survival Analysis and Radiosensitization Effects measurement	87
3.11	Combination Treatments Analysis of Synergism/Antagonism	88
3.12	Theoretical Dose Enhancement Factor Calculation	89
3.13	Post-irradiation ROS Measurement.....	91
3.14	Apoptosis Assay using Muse TM Flow Cytometry	92
3.15	Raman Spectroscopic Analysis.....	94
3.16	Statistical Analysis.....	97
CHAPTER 4 RESULTS		98
4.1	Cytotoxicity of BiONPs, Cis and BRF – Individually	98
4.1.1	Cell Viability against BiONPs.....	98
4.1.2	ROS Production against BiONPs	104
4.1.3	Cell Viability against Cisplatin (Cis)	107

4.1.4	Cell Viability against BRF	109
4.2	Cellular Uptake and Localization of BiONPs in Cells	111
4.2.1	Flow Cytometry Analysis.....	111
4.2.2	Microscopy Analysis	113
4.3	Cells Survival Curves and Sensitization Enhancement Ratio (SER)	114
4.3.1	Individual Treatment Components	114
4.3.1 (a)	^{192}Ir of γ -radiation.....	114
4.3.1 (b)	Photon Beam Therapy	116
4.3.1 (c)	Electron Beam Therapy	118
4.3.2	Combinatorial Treatment Components	121
4.3.2 (a)	^{192}Ir of γ -radiation.....	121
4.3.2 (b)	Photon Beam Therapy	123
4.3.2 (c)	Electron Beam Therapy	125
4.3.3	Combinatorial Treatment Analysis of Synergism/Antagonism	128
4.3.3 (a)	^{192}Ir of γ -radiation.....	129
4.3.3 (b)	Photon Beam Therapy	130
4.3.3 (c)	Electron Beam Therapy	131
4.4	Theoretical DEF Estimations.....	134
4.4.1	Theoretical DEF versus Experimental SER	136
4.5	Post-irradiation ROS Measurement.....	138
4.5.1	Individual Treatment Components	138
4.5.1 (a)	^{192}Ir of γ -radiation.....	138
4.5.1 (b)	Photon Beam Therapy	139
4.5.1 (c)	Electron Beam Therapy	141

4.5.2	Combinatorial Treatment Components	142
4.5.2 (a)	^{192}Ir of γ -radiation.....	142
4.5.2 (b)	Photon Beam Therapy	143
4.5.2 (c)	Electron Beam Therapy	144
4.5.3	Influence of Time on ROS Generation.....	146
4.5.3 (a)	^{192}Ir of γ -radiation.....	146
4.5.3 (b)	Photon Beam Therapy	147
4.5.3 (c)	Electron Beam Therapy	148
4.5.4	Influence of Beams Quality for BC Combination on ROS Generation	149
4.6	Apoptosis Analysis of BC Combination for ^{192}Ir of γ -radiation.....	150
4.7	Raman Spectroscopic Analysis of BC Combination for ^{192}Ir Source of Γ - radiation with the ^{192}Ir source	158
CHAPTER 5 DISCUSSIONS.....		164
5.1	Cytotoxicity of BiONPs, Cis and BRF – Individually	164
5.1.1	Cell Viability against BiONPs.....	164
5.1.2	ROS Production against BiONPs	168
5.1.3	Cell Viability against Cis.....	172
5.1.4	Cell Viability against BRF	173
5.2	Cellular Uptake and Localization of BiONPs in Cells	175
5.3	Radiosensitization Effects	179
5.3.1	Double Combination of Individual BiONPs, Cis or BRF with Radiation.....	179
5.3.1 (a)	BiONPs and Radiation.....	179
5.3.1 (b)	Cis and Radiation.....	184

5.3.1 (c)	BRF and Radiation	187
5.3.2	Combination of BC, BB or BCB with Radiation	190
5.3.3	Synergism, Additive or Antagonism (of Combination Treatments).....	195
5.4	Theoretical DEF vs. Experimental SER	199
5.5	ROS Measurement Post-irradiation.....	202
5.5.1	Individual Treatment Components	203
5.5.2	Combination Treatment Components.....	208
5.5.3	Influence of Time on ROS Generation.....	211
5.5.4	Influence of Beams Quality on ROS Generation in BC Combination	212
5.6	Apoptosis Mechanism in MCF-7 Cells after BC Combination and ¹⁹² Ir of γ -radiation Treatment.....	213
5.7	Biochemical Changes of MCF-7 Cells after BC Combination and ¹⁹² Ir of γ -radiation Treatment.....	217
CHAPTER 6 CONCLUSION.....		224
6.1	Summary of the Findings	224
6.1.1	Cytotoxicity of Individual Components: BiONPs, Cis and BRF	224
6.1.2	Radiosensitization Effects of Individual and Combination Treatments	224
6.1.3	ROS Measurement Post-irradiation.....	225
6.1.4	Apoptosis.....	226
6.1.5	Subcellular Biochemical Changes using Raman Spectroscopic Technique	226

6.2 Future Directions	226
REFERENCES.....	228
APPENDICES	
APPENDIX A: BiONPs DILUTIONS	
APPENDIX B: CIS MAIN STOCK CALCULATION	
APPENDIX C: BRFCONCENTRATION CALCULATION FOR CYTOTOXICITY ASSAY	
APPENDIX D: R ² VALUES OF EACH SURVIVAL CURVES BASED ON LQ MODEL	
APPENDIX E: COMPUSYN SOFTWARE PROTOCOL	
APPENDIX F: COMBINATION INDEX (CI) FOR THE ACTUAL EXPERIMENTAL POINTS	
APPENDIX G: RAMAN SPECTRAL DATA PRE-PROCESSING	
APPENDIX H: STATISTICAL TESTS FOR BEAM QUALITY ROS MEASUREMENT	
APPENDIX I: STATISTICAL TESTS FOR APOPTOSIS DATA	
APPENDIX J: FOLD CHANGES OF APOPTOTIC INDEX	
APPENDIX K: TURNITIN REPORT	
LIST OF PUBLICATIONS	

LIST OF TABLES

	Page
Table 2:1	Clinical categories of breast cancers23
Table 2:2	Types of breast cancers lines used in pre-clinical studies24
Table 2:3	Radiosensitization studies on Bi complexes in the current decade38
Table 2:4	IC ₅₀ values of cisplatin on several breast cancer cell lines.....43
Table 2:5	Examples of ROS inducers involved in cancer treatments55
Table 3:1	Different weight of Bi(NO ₃) ₃ .5H ₂ O and NaOH would influence the BiONPs sizes to be yielded 70
Table 3:2	Dilution techniques for the Cis final concentrations.76
Table 3:3	Treatment components for radiosensitization effect and ROS measurement studies.....83
Table 3:4	Calculated Z _{eff} for individual component.90
Table 4:1	Radiobiological analysis based on LQ models for Ir-192 of γ- radiation corresponding to Figure 4.12. 116
Table 4:2	Radiobiological analysis based on LQ models for photon beam therapy corresponding to Figure 4.13..... 118
Table 4:3	Radiobiological analysis based on LQ models for electron beam therapy corresponding to Figure 4.14..... 120
Table 4:4	Overall results of SER values by Individual Components 121
Table 4:5	Radiobiological analysis based on LQ models for Ir-192 of γ- radiation corresponding to Figure 4.15 123
Table 4:6	Radiobiological analysis based on LQ models for photon beam therapy corresponding to Figure 4.16..... 125
Table 4:7	Radiobiological analysis based on LQ models for electron beam therapy corresponding to Figure 4.17..... 127
Table 4:8	Overall results of SER values by Combinatorial Treatments..128
Table 4:9	The overall averages of CI values which are the indication of synergism (less than 0.9), additive (0.9 to 1.2), and antagonism (more than 1.2) effects..... 133
Table 4:10	Theoretical DEF values at 0.38 MeV and 2.0 MeV estimated from the Figure 4.21. The percentages were the ratio to the total volume in the cell suspensions. 136
Table 4:11	Stages of apoptosis after 14 hours treatment for the treatment of BC combination with Ir-192 of γ-radiation corresponding to Figure 4.35..... 154

Table 4:12	Stages of apoptosis after 40 hours treatment for the treatment of BC combination with Ir-192 of γ -radiation corresponding to Figure 4.36.....	157
Table 4:13	Detected peaks corresponded to Figure 4.38 and Figure 4.39.	162
Table 4:14	Assignment of Raman spectral peaks, based on the results reported in the literature and the present work, corresponding to Figure 4.38 and Figure 4.39.	163

LIST OF FIGURES

	Page
Figure 1.1	The current principles of radiobiology (Boustani et al., 2019; Chew et al., 2021; Cui, 2016; IAEA, 2017; Kesarwani et al., 2018; Mallick et al., 2020; Mayadev et al., 2017; “R,” 2017; Ramroth, 2017; Wray & Lightsey, 2016; Zoiopoulou, 2020). 7
Figure 1.2	Shapes of nanomaterials in the form of (A) dendrites, (B) cubes, (C) stars, (D) triangles, (E) cylinders and (F) spheres. Images are adapted from several published studies (Gratton et al., 2008; Lee et al., 2019; Muhammad et al., 2018; Xie et al., 2017). 10
Figure 1.3	Classical radiosensitization process in the presence of therapeutic NPs in RT for cancer treatment. The figure is adapted from Yan Liu et al. (2018). 11
Figure 2.1	Stages of breast cancers according to the tumor sizes. Illustration was adapted from Breast Cancer Now Ltd. (2018) 22
Figure 2.2	The typical surviving curves fitted to the LQ model indicated the chronic line (for normal cells) and acute line (for cancer cells). The picture is taken from Mayadev et al. (2017). 32
Figure 2.3	The surviving curves fitted to LQ model depicts the areas of one-hit event (α component) two-hit event event (β component). The dotted line shows the α / β ratio line. The graph is taken from McMahon & Prise (2019). 33
Figure 2.4	The energies of the incident photon ($h\nu$) are fully absorbed by the NPs at the low energies, and partially absorbed by the NPs at the high energies. The electrons (e^-) released by the interactions would induce DNA damages to the cells. 35
Figure 2.5	Leaves of the OI plant 49
Figure 2.6	Regulation of genes and proteins expression (increase in red bubbles, decrease in blue bubbles) in cancer cells after treatment with OI plant extract or baicalein, leading to the disruption of the cell cycle as well as metastasis and finally causing autophagic or apoptotic cell death. 52
Figure 2.7	Morphological changes of cells in apoptosis processes after treatments, which involved the six characteristics, referred to IAEA (2017) and K. K. Jain (2008). 58
Figure 3.1	The brief flow chart of the research methodology. The study into three phases, such as biocompatibility, radiosensitization and mechanism of action studies. 67
Figure 3.2	Flow processes of the BiONPs synthesis. The protocols were reported in previous literatures (Zainal Abidin, 2019; Zulkifli, Razak, Rahman, et al., 2018). 69

Figure 3.3	(A) The stirring of the dilution of $\text{Bi}(\text{NO}_3)_3 \cdot 5\text{H}_2\text{O}$ and Na_2SO_4 in distilled water (B) The yellow precipitate resultants in Schott bottle sealed for hydrothermal reaction.	69
Figure 3.4	The processes of obtaining BRF from OI plant leaves, referred to Wahab and Mat (2018).	71
Figure 3.5	Images of the three cell lines that were used in this study, fixed using cold methanol and stained with 1% of crystal violet solution.	73
Figure 3.6	Calculation of BiONPs stock solution.	74
Figure 3.7	The method to measure the intracellular ROS generation. Protocols were modified from Yan Li et al. (2010) and Hui Yang et al. (2009).	79
Figure 3.8	Protocol developed in the present study for the BiONPs intracellular localization for observation under the light microscope.	80
Figure 3.9	Quantitative measurement of BiONPs cellular uptake by flow cytometry, referred to Reineke (2012).	81
Figure 3.10	Set up for Ir-192 of γ -radiation with (A) upper view and (B) lateral view. (C) The connection between the HDR machine to the surface mold on the table couch. (D) Schematic diagram of the set up.	84
Figure 3.11	Set up of irradiation in (A) real view and (B) schematic diagram for the photon beam therapy.	85
Figure 3.12	Set up of irradiation in (A) real view and (B) schematic diagram for the electron beam therapy with an applicator.	86
Figure 3.13	The arrangement for the irradiations in 6-wells plates involved row A which was reserved for control cells and row B which was reserved for the BC treatment component in triplicates.	93
Figure 3.14	The Muse TM Cell Analyzer used for apoptosis assay.	93
Figure 3.15	(A) Renishaw InVia Raman Microscope was used for this study. (B) Glass coverslips with cells attached were put on a borosilicate float glass microscope slide with aluminium metal coating under microscope lens, as shown by the red arrow.	96
Figure 3.16	The schematic diagram of the point of analysis using Raman Microscope, which was centered at the nucleoli of the cell.	96
Figure 4.1	Cell viabilities after treatment with BiONPs of 60 nm diameter size with five concentrations for 24, 48 and 72 hours on MCF-7, MDA-MB-231 and NIH/3T3 cell lines, respectively. The dashed lines marked 80% of the cell viability. Each error bar represents the standard error of the mean (SEM).	99
Figure 4.2	Cell viabilities after treatment with BiONPs of 70 nm diameter size with five concentrations for 24, 48 and 72 hours on MCF-7, MDA-MB-231 and NIH/3T3 cell lines, respectively. The dashed	

	lines marked 80% of the cell viability. Each error bar represents the SEM.	100
Figure 4.3	Cell viabilities after treatment with BiONPs of 80 nm diameter size with five concentrations for 24, 48 and 72 hours on MCF-7, MDA-MB-231 and NIH/3T3 cell lines, respectively. The dashed lines marked 80% of the cell viability. Each error bar represents the SEM.	102
Figure 4.4	Cell viabilities after treatment with BiONPs of 90 nm diameter size with five concentrations for 24, 48 and 72 hours on MCF-7, MDA-MB-231 and NIH/3T3 cell lines, respectively. The dashed lines marked 80% of the cell viability. Each error bar represents the SEM.	103
Figure 4.5	Detection of DCF percentages after treatment with four different BiONPs sizes (60, 70, 80 and 90 nm) of the 0.5 mM of BiONPs immediately after treatment (0-1 h), 3.5, 6 and 24 hours in MCF-7, MDA-MB-231 and NIH/3T3 cell lines respectively. The treated cells were compared to control cells treated with DCH ₂ F-DA only (positive control), 100 % DCF fluorescent. Each error bar represents the SEM, but in this figure they are too small..	105
Figure 4.6	Detection of DCF percentages after treatment with five concentrations of the BiONPs of 60 nm diameter size immediately after treatment (0-1 h), 3.5, 6 and 24 hours in MCF-7, MDA-MB-231 and NIH/3T3 cell lines respectively. The treated cells were compared to control cells treated with DCH ₂ F-DA only (positive control), 100% DCF fluorescent. Each error bar represents the SEM.....	107
Figure 4.7	Colour changes of the culture media at 4 hours after adding the Prestoblue reagent to the cells in the wells. The arrangement of Cis or BRF treatment in the 96 wells plate started with C as the control row and followed by the treatments on cells with the highest concentration (1) to the lowest concentration (9).	108
Figure 4.8	Cis cytotoxic evaluation against MCF-7, MDA-MB-231, and NIH/3T3 cell lines. Each point shows the average percentage of viable cells in comparison to the negative control. The dashed lines represent the IC ₂₅ and IC ₅₀ levels, respectively. Curves are fitted using the Dose-Response model. Error bars represent the SEM.....	109
Figure 4.9	Cytotoxic evaluation of BRF against MCF-7, MDA-MB-231, and NIH/3T3 cell lines. Each point shows the average percentage of viable cells in comparison to the negative control. Dashed lines represent the IC ₂₅ and IC ₅₀ levels. Curves are fitted using the Dose-Response model. Error bars represent the SEM.	110
Figure 4.10	Cell population detected by flow cytometric analysis on MCF-7, MDA-MB-231 and NIH/3T3 cell lines after the introduction of the 60 nm of BiONPs with 0.5 mM concentration, relative to the control. Each percentage represent the average of triplicate samples.	112

Figure 4.11	Localization of BiONPs close to nuclei in the (A) MCF-7, (B) MDA-MB-231 and (C) NIH/3T3 cells, after 24 hours incubation with the BiONPs. Arrows indicated the rod-shaped BiONPs presented in the cells. The scale of each picture is 20 μm	113
Figure 4.12	The cell survival curves of the MCF-7, MDA-MB-231 and NIH/3T3 cell lines after Ir-192 of γ -radiation at 0 to 4 Gy of doses in the presence of BiONPs (red line), Cis (blue line), BRF (green line) and the control (black line). The survival data were fitted to LQ models. Error bars represent the standards errors of survival fractions.	115
Figure 4.13	The cell survival curves of the MCF-7, MDA-MB-231 and NIH/3T3 cell lines after photon beam therapy at 0 to 10 Gy of doses in the presence of BiONPs (red line), Cis (blue line), BRF (green line) and the control (black line). The survival data were fitted to LQ models. Error bars represent the standards errors of survival fractions.	117
Figure 4.14	The cell survival curves of the MCF-7, MDA-MB-231 and NIH/3T3 cell lines after electron beam therapy at 0 to 10 Gy of doses in the presence of BiONPs (red line), Cis (blue line), BRF (green line) and the control (black line). The survival data were fitted to LQ models. Error bars represent the standards errors of survival fractions.	119
Figure 4.15	The cell survival curves of the MCF-7, MDA-MB-231 and NIH/3T3 cell lines after Ir-192 of γ -radiation at 0 to 4 Gy of doses in the presence of BC (red line), BB (blue line), BCB (green line) and the control (black line). The survival data were fitted to LQ models. Error bars represent the standards errors of survival fractions.	122
Figure 4.16	The cell survival curves of the MCF-7, MDA-MB-231 and NIH/3T3 cell lines after photon beam therapy at 0 to 10 Gy of doses in the presence of BC (red line), BB (blue line), BCB (green line) and the control (black line). The survival data were fitted to LQ models. Error bars represent the standards errors of survival fractions.	124
Figure 4.17	The cell survival curves of the MCF-7, MDA-MB-231 and NIH/3T3 cell lines after electron beam therapy at 0 to 10 Gy of doses in the presence of BC (red line), BB (blue line), BCB (green line) and the control (black line). The survival data were fitted to LQ models. Error bars represent the standards errors of survival fractions.	126
Figure 4.18	The F_a -CI plots of BC (blue), BB (red), and BCB (green) combination treatments in MCF-7, MDA-MB-231 and NIH/3T3 cells for γ -radiation with the Ir-192 source. Each point is the CI values of the actual combination data point, and the lines are the simulated CI values.	130
Figure 4.19	The F_a -CI plots of BC (blue), BB (red), and BCB (green) combination treatments in MCF-7, MDA-MB-231 and NIH/3T3	

	cells for photon beam therapy. Each point is the CI values of the actual combination data point, and the lines are the simulated CI values.....	131
Figure 4.20	The F_a -CI plots of BC (blue), BB (red), and BCB (green) combination treatments in MCF-7, MDA-MB-231 and NIH/3T3 cells for electron beam therapy. Each point is the CI values of the actual combination data point, and the lines are the simulated CI values.....	132
Figure 4.21	Theoretical DEF of each treatment component (BiONPs, Cis, BRF, BC, BB and BCB) at (A) various energy ranges, (B) Ir-192 of γ -radiation average energy of 0.38 MeV, and (C) 6 MV photon beam with an effective energy of 2 MeV. The percentage of each component depended on the volume of the treatment components used during the irradiation.....	135
Figure 4.22	Comparison of theoretical DEF values and experimental SER values by each treatment component for Ir-192 of γ -radiation in MCF-7, MDA-MB-231, and NIH/3T3 cells. Theoretical DEF values are obtained from Table 4:10, and experimental SER values are acquired from Table 4:4 and Table 4:8.	137
Figure 4.23	Comparison of theoretical DEF values and experimental SER values by each treatment component for photon beam therapy in MCF-7, MDA-MB-231, and NIH/3T3 cells. Theoretical DEF values are obtained from Table 4:10, and experimental SER values are acquired from Table 4:4 and Table 4:8.	138
Figure 4.24	Percentage of ROS generation immediately after (0 hour) the γ -radiation with the Ir-192 source at doses of 0, 3 and 6 Gy in MCF-7, MDA-MB-231, and NIH/3T3 cell lines treated with BiONPs, BRF and Cis. Error bars represent the SEM.....	139
Figure 4.25	Percentage of ROS generation immediately after (0 hour) the photon beam irradiation at doses of 0, 3 and 6 Gy in MCF-7, MDA-MB-231, and NIH/3T3 cell lines treated with BiONPs, BRF and Cis. The y-axis scale of ROS Generation (%) of NIH/3T3 cell graph differed from the graphs of MCF-7 and MDA-MB-231 cells. Error bars represent the SEM.....	140
Figure 4.26	Percentage of ROS generation immediately after (0 hour) the electron beam irradiation at doses of 0, 3 and 6 Gy in MCF-7, MDA-MB-231, and NIH/3T3 cell lines treated with BiONPs, BRF and Cis. The y-axis scale of ROS Generation (%) of NIH/3T3 cell graph differed from the graphs of MCF-7 and MDA-MB-231 cells. Error bars represent the SEM.....	141
Figure 4.27	Percentage of ROS generation immediately after (0 hour) γ -radiation with the Ir-192 source at doses of 0, 3 and 6 Gy in MCF-7, MDA-MB-231, and NIH/3T3 cell lines treated with BC, BB, and BCB combinations. Error bars represent the SEM.....	142
Figure 4.28	Percentage of ROS generation immediately after (0 hour) the photon beam irradiation at doses of 0, 3 and 6 Gy in MCF-7,	

	MDA-MB-231, and NIH/3T3 cell lines treated with BC, BB, and BCB combinations. The y-axis scale of ROS Generation (%) of NIH/3T3 cell graph differed from the graphs of MCF-7 and MDA-MB-231 cells. Error bars represent the SEM.....	143
Figure 4.29	Percentage of ROS generation immediately after (0 hour) the electron beam irradiation at doses of 0, 3 and 6 Gy in MCF-7, MDA-MB-231, and NIH/3T3 cell lines treated with BC, BB, and BCB combinations. The y-axis scale of ROS Generation (%) of NIH/3T3 cell graph differed from the graphs of MCF-7 and MDA-MB-231 cells. Error bars represent the SEM.....	145
Figure 4.30	Percentage of ROS generation increments immediately after (0 h), 3 hours and 24 hours after γ -radiation with the Ir-192 source with only a dose of 6 Gy in MCF-7, MDA-MB-231, and NIH/3T3 cell which were treated with the BiONPs, BRF, Cis, BC, BB, and BCB, relative to the positive control. Error bars represent the SEM.....	147
Figure 4.31	Percentage of ROS generation increments immediately after (0 h), 3 hours and 24 hours after photon beam therapy with only a dose of 6 Gy in MCF-7, MDA-MB-231, and NIH/3T3 cell which were treated with the BiONPs, BRF, Cis, BC, BB, and BCB, relative to the positive control. The y-axis scale of ROS Generation (%) of NIH/3T3 cell graph differed from the graphs of MCF-7 and MDA-MB-231 cells. Error bars represent the SEM.....	148
Figure 4.32	Percentage of ROS generation increments immediately after (0 h), 3 hours and 24 hours after electron beam therapy with only a dose of 6 Gy in MCF-7, MDA-MB-231, and NIH/3T3 cell which were treated with the BiONPs, BRF, Cis, BC, BB, and BCB, relative to the positive control. Error bars represent the SEM.....	149
Figure 4.33	A review of the percentages of ROS generation in the presence of BC combination for all the radiation beams. Error bars represent the SEM.	150
Figure 4.34	Overall cell population profile detected by flow cytometric analysis on MCF-7 cells of control and BC treatment after 14 hours (14h) and 40 hours (40h) of Ir-192 of γ -radiation irradiation. Each box is gated by cell size index and Annexin V agent detections.	152
Figure 4.35	Apoptosis profile from the flow cytometric analysis on MCF-7 cells of control (left column) and BC combination treatment (right column) after 14 hours of γ -radiation with the Ir-192 source with doses of 0, 2 and 4 Gy. Each box is gated by cell viability (7-AAD) agent and Annexin V agent detections. The percentages in the figure represent one sample only, but the average percentage of the three samples is tabulated in Table 4:11.	153
Figure 4.36	Apoptosis profile from the flow cytometric analysis on MCF-7 cells of control (left column) and BC combination treatment (right column) after 40 hours of γ -radiation with the Ir-192 source with	

	doses of 0, 2 and 4 Gy. Each box is gated by cell viability (7-AAD) agent and Annexin V agent detections. The percentages in the figure represent one sample only, but the average percentage of the three samples is tabulated in Table 4:12 156
Figure 4.37	Label-free imaging by Raman microscopy of control and BC-treated MCF-7 cells fixed at 0- and 24-hours after γ -radiation with the Ir-192 source, with the nucleoli as the region of interests at the center for analysis. White arrows indicate the BiONPs presence in the cells, while yellow arrows show the cellular membrane damages. The scales of each picture are 20 μm 158
Figure 4.38	Average Raman spectrum of about three single MCF-7 cells immediately after (0 hour) γ -radiation with the Ir-192 source with doses of 0, 0.5 and 2 Gy for control (dashed lines) and BC combination treatment (solid lines). The labels refer to the wavenumber value and attribution of the most critical spectral features. The zoomed-in area ranged from 1100 to 1300 cm^{-1} 160
Figure 4.39	Average Raman spectrum of about three single MCF-7 cells at 24 hours γ -radiation with the Ir-192 source with doses of 0, 0.5 and 2 Gy for control (dashed lines) and BC combination treatment (solid lines). The labels refer to the wavenumber value and attribution of the most critical spectral features. The zoomed-in area ranged from 1100 to 1300 cm^{-1} 161
Figure 5.1	The structural changes in cells detected by Raman spectroscopic analysis. 223

LIST OF ACRONYMS, ABBREVIATIONS AND SYMBOLS

%	Percent
°C	Degree Celsius
μ	Micro
•OH	Hydroxyl radicals
¹⁰³ Pd	Palladium-103
¹²⁵ I	Iodine-125
¹³⁷ Cs	Cesium-137
¹⁶⁹ Yb	Ytterbium-169
¹⁹² Ir or Ir-192	Iridium-192
2D	2-dimentional
3D	3-dimentional
5-ALA	5-Aminolevulinic acid
⁶⁰ Co	Cobalt-60
7-AAD	7-aminoactinomycin D
AMPK	5' adenosine monophosphate-activated protein kinase
ATP	Adenosine triphosphate
Bax	Bcl2 Associated X-protein
BB	BiONPs-BRF
BC	BiONPs-Cis
BCB	BiONPs-Cis-BRF
Bcl2	B-cell lymphoma 2
Bi	Bismuth
Bi (NO ₃) ₃ .5H ₂ O	Bismuth (III) nitrate pentahydrate

Bi ₂ O ₃	Bismuth oxide
Bi ₂ S ₃	Bismuth sulfide
Bi ₂ Se ₃	Bismuth selenide
BiFeO ₃	Bismuth ferrite
BiONPs	Bismuth oxide nanoparticles
BiP ₅ W ₃₀	Bismuth heteropoly tungstate
BRF	Baicalein-rich fraction
C	Carbon
CDK	Cyclin-dependent kinase
CI	Combination index
Cis	Cisplatin
CK2	Casein kinase 2
cm	Centimeter
CO ₂	Carbon dioxide
CRT	Chemoradiotherapy
CT	Computed tomography
Cyt	Cytosine
DCF	2',7'-dichlorofluorescein
DCH ₂ F-DA	2',7'- dichlorodihydro-fluorescein diacetate
DCIS	Ductal carcinoma in situ
DEF	Dose enhancement factor
DIABLO	Direct IAP Binding protein with Low pi
d _{max}	Depth of maximum dose
DMEM	Dulbecco's Modified Eagles Medium
DMF	Dose modifying factor

DMSO	Dimethyl sulfoxide
DNA	Deoxyribonucleic acid
Drp1	Dynamin-related protein 1
EMT	Epithelial-mesenchymal transition
ER	Estrogen receptor
ERK	Extracellular receptor kinases
F _a	Fraction affected
FA	Folic acid
Fas	Fas cell surface death receptor
FasL	Fas ligand
FBS	Fetal bovine serum
G1 phase	Growth phase 1
G2 phase	Growth phase 2
G3BP1	GTPase-activating protein-binding protein
GI ₅₀	Concentration which induced 50% of growth inhibition
GLP	<i>Ganoderma lucidum</i> polysaccharide
GPx	Glutathione peroxidase
GSK-3β	Glycogen synthase kinase 3β
GTP	Guanosine triphosphate
Gy	Gray (unit of radiation dose)
H	Hydrogen
H ₂ O ₂	Hydrogen peroxide
HDR	High dose rate
HER2	Human epidermal growth factor receptor 2
Hes	Hairy/Enhancer of split

HIF	Hypoxia-inducible factor
HO-1	Heme oxygenase-1
HRS	Hormone receptor sensitive
IAEA	International Atomic Energy Agency
IARC	International Agency for Research on Cancer
IC ₂₅	Inhibition concentration which causes 25% cell death
IC ₅₀	Inhibition concentration which causes 50% cell death
IL	Interleukin
JNK	c-Jun NH2-terminal kinase
kV	Kilovoltage
kVp	Kilovoltage peak
LET	Linear energy transfer
LQ	Linear quadratic
M phase	Mitosis phase
MAPKs	Mitogen-activated protein kinases
MeV	Mega electron-volt
ml	Millimeter
mMol/L	Milli mol per liter
mM	Millimolar
MMP	Matrix metalloproteinase
MNCR	Malaysia National Cancer Registry
MONPs	Metal oxide NPs
mRNA	Messenger RNA
MT	Multitarget
mTOR	Mammalian target of rapamycin

MTT	3- [4,5-dimethylthiazol-2- yl]-2,5-diphenyl tetrazolium bromide
MV	Megavoltage
Na ₂ SO ₄	Sodium sulphate
NaOH	Sodium hydroxide
NCI	National Cancer Institute
NF-κB	Nuclear factor kappa B
NIH	National Institute of Health
nm	Nanometer
NOX	Nicotinamide adenine dinucleotide phosphate oxidase
NPC	Nuclear pore complex
NPs	Nanoparticles
Nrf	nuclear factor E2-related factor 2
O ₂ • ⁻	Superoxide radicals
OI	<i>Oroxylum indicum</i>
p53	Protein 53
PARP	Poly-ADP-ribose polymerase
PBS	Phosphate buffered saline
PEG	Polyethylene glycol
Phe	Phenylalanine
PO ₂ ⁻	Phosphodioxy bond of phosphate
PR	Progesterone receptor
pRb	Retinoblastoma protein
PTP1B	protein tyrosine phosphatase 1B
Q	Quadrant
RAP80	Receptor-associated protein 80

RBE	Relative biological effectiveness
RCR	Repairable conditionally repairable
redox	Reduction-oxidation
RNA	Ribonucleic acid
ROS	Reactive oxygen species
RS	Raman spectroscopy
RT	Radiotherapy
S phase	DNA synthesis phase
SEM	Standard error of the mean
SER	Sensitization enhancement ratio
SESN	Sestrins
SF	Survival fraction
SLC	Solute carries
SLD	Sublethal damage
SMAC	Mitochondria-derived activator of caspase
SNHG	Small nucleolar RNA host gene
SOD	Superoxide dismutase
SPIONs	Superparamagnetic iron oxide NPs
SSD	Source-to-surface distance
STAT3	Signal transducer and activator of transcription 3
TLC	Thin layer chromatography
TNF	Tumor necrosis factor
TRAF2	Tumor necrosis factor receptor-associated factor 2
TRAIL	Tumor necrosis factor-related apoptosis-inducing ligand
Tyr	Tyrosine

WHO	World Health Organization
XIAP	X-linked inhibitor of apoptosis protein
Z	Atomic number
ZEB1-AS1	Zinc finger E-box binding homeobox 1 antisense 1
Z_{eff}	Effective atomic number
α	Alpha
β	Beta
γ	Gamma
γ H2AX	γ -H2A histone family member X

**KESAN RADIOSENSITIVITI BERPENSINERGI DARIPADA GABUNGAN
NANOPARTIKEL BISMUT OKSIDA, CISPLATIN DAN FRAKSI KAYA-
BAICALEIN DARIPADA *Oroxylum indicum* UNTUK RADIOTERAPI
KLINIKAL**

ABSTRAK

Strategi multimod bagi rawatan kanser bertujuan untuk menghapuskan penyakit barah yang kompleks dengan menggunakan peningkatan hasil terapi melalui efek gabungan berbanding dengan teknik berasingan yang mungkin mempunyai beberapa had. Ubat kemoterapi seperti cisplatin dapat meningkatkan dos sinaran pada tisu sasaran. Walau bagaimanapun, ketoksikan ubat-ubatan komersil telah mendorong para penyelidik untuk mencari agen alternatif dan pemeka sinaran tanpa toksin, kemungkinan daripada derivatif semula jadi atau nanopartikel (NPs) yang berasaskan logam. Kajian ini bertujuan untuk menyelidik kesan radiosensitiviti sinergi oleh NPs bismut oksida (BiONPs), cisplatin (Cis) dan fraksi kaya-baicalein (BRF) daripada ekstrak daun *Oroxylum indicum* (OI) di bawah radioterapi klinikal menggunakan brakiterapi dengan kadar dos tinggi (HDR), pancaran foton, dan pancaran elektron. Kesitotoksikan, pengambilan ke dalam sel, dan pengeluaran spesies oksigen reaktif (ROS) yang disebabkan oleh BiONPs dikaji ke atas sel kanser payudara MCF-7 dan MDA-MB-231 serta sel normal fibroblas NIH/3T3 bagi menerangkan kebolegunaan BiONPs dalam aplikasi radioterapi. Kepekatan Cis dan BRF yang selamat juga telah ditentukan sebelum iridiasi. Pengkuantitian kesan radiosensitiviti dan penjanaan ROS dikaji dengan BiONP, Cis, dan BRF individu, serta kombinasi BiONPs-Cis (BC), BiONPs-BRF (BB) dan BiONPs-Cis-BRF (BCB) bagi brakiterapi HDR, pancaran foton, dan pancaran elektron. Analisis spektroskopi Raman dan apoptosis dilakukan

untuk menjelaskan perubahan biokimia subselular dan mekanisme kematian sel. Hasil kesitotoksikan menunjukkan bahawa BiONPs telah menyebabkan kematian sel yang minimum kurang daripada 20% secara purata, sementara nilai pengeluaran ROS oleh BiONPs boleh diabaikan. Peningkatan pengambilan NPs ke dalam sel menunjukkan bahawa BiONPs boleh disebatikan dan juga melekat pada permukaan sel. Demikian itu, didapati bahawa 0.5 mM dari 60 nm BiONPs adalah kepekatan dan saiz optima untuk aplikasi radioterapi. Nilai terendah bagi 25% kepekatan perencatan oleh individu Cis dan BRF yang diperoleh adalah masing-masing 1.30 μM dan 0.76 $\mu\text{g/ml}$, dan nilai ini digunakan untuk eksperimen seterusnya. Siasatan kesan radiosensitiviti antara komponen-komponen rawatan menunjukkan nilai nisbah peningkatan sensitiviti (SER) tertinggi adalah menggunakan gabungan BC dalam sel MCF-7, diikuti oleh rawatan BCB dan BB. Kesannya lebih ketara untuk brakiterapi HDR berbanding pancaran foton dan elektron. Sementara itu, rawatan gabungan telah menyebabkan tahap ROS yang lebih tinggi untuk pancaran foton berbanding brakiterapi dan pancaran elektron. Peningkatan ROS tertinggi adalah disebabkan oleh gabungan BC dalam sel MDA-MB-231. Menariknya, gabungan BCB juga memberikan nilai SER yang tinggi tetapi secara kolektifnya turut mempengaruhi sel normal. Gabungan BC dalam sel MCF-7 telah menunjukkan potensi sebagai pemeka sinaran yang berkesan untuk brakiterapi dengan kejadian proses apoptosis awal, terutamanya dalam masa 40 jam selepas radiasi. Penemuan dari spektroskopi Raman menunjukkan bahawa gabungan BC dan brakiterapi akan mempengaruhi proses glikolisis, susunan struktur asid amino dan kestabilan DNA/RNA yang menyaranakan peningkatan kesan radiasi pada sel-sel kanser. Kesimpulannya, kajian ini menunjukkan potensi BiONP, Cis dan BRF sebagai pemeka sinaran yang dapat memperbaiki kecekapan radioterapi untuk menghapuskan sel-sel kanser. Gabungan

pemeka sinaran yang poten ini mungkin dapat menghasilkan kesan sinergi yang akan menambahkan impak dalam radioterapi secara klinikal.

**SYNERGETIC RADIOSENSITIZATION EFFECTS OF BISMUTH OXIDE
NANOPARTICLES, CISPLATIN AND BAICALEIN-RICH FRACTION
FROM *Oroxylum indicum* COMBINATIONS FOR CLINICAL
RADIOTHERAPY**

ABSTRACT

Multimodal strategies of cancer treatment aim to eradicate complex malignant disease with enhanced therapeutic outcome with combined synergetic effects in contrast to individual techniques that might exhibits some limitations. Chemotherapeutic drug such as cisplatin have been applied to increase radiation doses at target tissues in radiotherapy. However, commercial chemo-drugs toxicities had compelled the researchers to evaluate alternatives for non-toxic agents and radiosensitizers, potentially from natural derivatives or metal-based nanoparticles (NPs). Integration of novel nanomaterials and natural product as radiosensitizer to increase the anti-tumors efficacy are also promising to enhance the treatment performance. This study aimed to investigate the synergetic radiosensitization effects of bismuth oxide NPs (BiONPs), cisplatin (Cis) and a baicalein-rich fraction (BRF) from *Oroxylum indicum* (OI) leaves extract under clinical radiotherapy of High Dose Rate (HDR) brachytherapy, photon, and electron beams. The cytotoxicity, cellular uptake, and reactive oxygen species (ROS) generation induced by BiONPs were initially investigated on MCF-7 and MDA-MB-231 breast cancer as well as NIH/3T3 normal fibroblast cell lines in elucidating the BiONPs feasibility for radiotherapy application. The safe concentration of Cis and BRF were also determined prior irradiation. Quantification of radiosensitization effects and ROS generation were conducted with individual BiONPs, Cis, and BRF, as well as BiONPs-Cis (BC),

BiONPs-BRF (BB) and BiONPs-Cis-BRF (BCB) combinations for High Dose Rate (HDR) brachytherapy, photon, and electron beams. Raman Spectroscopy and apoptosis analysis were conducted to elucidate the subcellular biochemical changes and cells death mechanism. The cytotoxicity results provide that the BiONPs induced minimal cell deaths constituting less than 20% on average while ROS production by BiONPs was negligible. The increment of NPs cellular uptake indicated that BiONPs were internalized and bound to the cellular surfaces. Consequently, 0.5 mM of 60 nm BiONPs was found to be an optimum concentration and size for radiotherapy application. The lowest values of the 25% of inhibition concentration by individual Cis and BRF obtained were 1.30 μ M and 0.76 μ g/ml, respectively, and utilized for the subsequent experiments. Investigation of the radiosensitization effects among the treatment components indicated the highest SER value by BC combination in MCF-7 cells, followed by BCB and BB treatments. The effects were more prominent for Ir-192 of γ -radiation compared to photon and electron beams. Meanwhile, the combination treatments present the higher ROS levels for photon beam than brachytherapy and electron beam. The highest ROS enhancement was attributed to the presence of BC combination in MDA-MB-231 cells. Interestingly, the BCB combination also showed a high SER but collaterally affected the normal cells. The BC combination of MCF-7 cells showed potential as an effective radiosensitizer for brachytherapy with the early apoptosis predominantly occurred within 40 hours after irradiation. Finally, the finding from Raman spectroscopy demonstrated that the BiONPs-Cis and brachytherapy combination would affect the glycolysis process, the amino acid structure arrangement and the DNA/RNA stability that would suggest the enhancement of radiation effects on cancer cells. In conclusion, this study suggests the potential of BiONPs, Cis and BRF as radiosensitizer that could improve the efficiency

of radiotherapy to eradicate the cancer cells. The combination of these potent radiosensitizers could produce synergetic effects that will elevate the therapeutic impact of clinical radiotherapy.

CHAPTER 1

INTRODUCTION

1.1 Introduction to Radiotherapy

Radiotherapy (RT) is one of the cancer treatments, apart from surgery, chemotherapy, immunotherapy, hormone therapy, targeted therapy, stem cell transplant and precision medicine, as listed by the International Agency for Research on Cancer (IARC) and the National Cancer Institute (NCI) (IARC, 2014; NCI, 2020). The International Atomic Energy Agency (IAEA) also stated that RT can be administered alone or in combination with chemotherapy, as well as after surgery in the cancer treatment plans (IAEA, 2017). RT uses high energy ionizing radiation to manage and treat cancer diseases as well as some other non-malignant conditions (“R,” 2017). Nowadays, there are approximately 7600 RT centers around the world (IAEA, 2017). Meanwhile in Malaysia, there are currently 30 RT centers with approximately 58 megavoltage machines, in several states such as Federal Territory of Kuala Lumpur, Feral Territory of Putrajaya, Selangor, Kelantan, Sarawak, Sabah, Perak, Penang, Malacca and Negeri Sembilan (Yahya et al., 2019).

Ionizing radiation started to be used as a therapy in cancer care since Curie's discovery of radium by 1898 and its successful treatment on cervical cancer in 1905, which was the foundation for brachytherapy (IAEA, 2017). Later, the external beam source was standardized in 1976 for clinical RT practice (IAEA, 2017). There are two major types of RT available which are the external beam therapy (electron or photon beams) and the internal therapy (brachytherapy) (NCI, 2020).

The external beam is generated from a megavoltage (MV) machine known as the medical linear electron accelerator (linac), replacing the old cobalt-60 (^{60}Co)

teletherapy machine (IAEA, 2017). The MV machine uses a current of fast traveling subatomic particles that were formed by electricity or high-frequency electromagnetic waves, creating the high energy of electron radiation. (IAEA, 2017; Khan, 2014). In addition, the X-ray photon beam could also be supplied from the linac via Bremsstrahlung phenomena, a braking process which deflects the electrons from the original path (Khan, 2014; “Radiation in Bioanalysis Spectroscopic Techniques and Theoretical Methods,” 2019). The linac has a gantry which could operate at a 360-degree rotation to deliver the radiations to a targeted body part from many directions (IAEA, 2017; NCI, 2020). The photon and electron beams are used in RT for cancers in different positions. Electron beam with energies up to 21 MeV is usually used for superficial tumors, while the photon beam is used for deep-seated tumors (Abidin, Zulkifli, et al., 2019; Raizulnasuha Ab Rashid et al., 2017; Wilkens, 2007).

In contrast, brachytherapy is a highly localized treatment in which radioactive sources are delivered near to the target sites internally, thus providing a high dose of gamma (γ)-energy radiation to the cancer cells while conserving electrical energy (IAEA, 2017; Wan Nordiana Wan Abdul Rahman, 2010). Originally, radon dan radium sources were used for the brachytherapy, but nowadays, the common isotopes that are used included Cesium-137 (^{137}Cs), Iridium-192 (^{192}Ir or Ir-192), Gold-198 (^{198}Au), Iodine-125 (^{125}I), and Palladium-103 (^{103}Pd) (Khan, 2014). The physical properties of the radionuclides also offer some advantages relative to the external beams, in terms of source size, γ -energy, source half-life, and flexibility (Khan, 2014). The brachytherapy is usually utilized for the treatment of prostate cancer and gynecological cancers as well as vascular disease (Khan, 2014).

1.2 Radiosensitization Mechanisms

Irrespective of the types of radiation, the mechanism of cell death after ionizing radiation involved a sequential physical, chemical, and biological effects (Brun & Sicard-Roselli, 2016). Firstly, physical interactions between the radiation and matters, concerning the energy absorption, were initiated in a few femtoseconds (McMahon & Prise, 2019; Mondelaers & Lahorte, 2001). After that, the chemical process occurred for a few nanoseconds, comprised of the energy transfer and reactions among the radiation-induced chemicals and some biological intermediates (McMahon & Prise, 2019; Mondelaers & Lahorte, 2001). The afterward short- and long-term biological responses that could pertain for hours, days, weeks or years after the radiation exposure would modify the cellular and tissue mechanisms (McMahon & Prise, 2019; Mondelaers & Lahorte, 2001).

1.2.1 Physical Phase

The physical phase is an interval period in which the high-energy particles pass through the target medium and instigate the energy absorption as well as the ionization or excitation of the matter (Cui, 2016; Mondelaers & Lahorte, 2001). The high-energy particles may consist of neutrons, and photons from X-rays and γ -radiation, as well as charged particles (electron, α - and β -particles) (Mondelaers & Lahorte, 2001). The high-energy charged particles are termed as direct ionizing particles as it can be considered as primary irradiation itself (Mondelaers & Lahorte, 2001). Meanwhile, the photons and neutrons were considered as indirect ionizing radiations due to the induction of secondary electrons from the sources (Mondelaers & Lahorte, 2001).

The high energy radiation will be absorbed and transferred to non-bonding or π -bonding atomic electrons of the other elements such as oxygen and nitrogen or other compounds (Mondelaers & Lahorte, 2001). The process can be measured as linear energy transfer (LET), in which the energy lost per length of the particles' track and absorbed in the medium (Mallick et al., 2020; Zeman et al., 2016). The LET level depends on the medium density, as well as the types and velocity of the primary radiation (Mondelaers & Lahorte, 2001). Neutrons and heavy ions are the high LET radiations, while X-rays and electrons are the low LET radiations (Zeman et al., 2016). High LET radiations will stimulate a high amount of excitation and ionizations per unit of tissue traversed, which also linearly proportional to relative biological effectiveness (RBE) and the number of cell killed (IAEA, 2017).

In this phase, the physical enhancement could also happen. It is defined as the boost of the electrons energy that were released back from the other matter present, such as nanoparticles, after the absorption (T. Guo, 2019). The physical enhancement, for instance from a few eV to tens of keV, could be calculated by comparing the energy deposition in the samples with nanomaterials relative to the samples without it (T. Guo, 2019). The energy from the secondary electrons released from the nanomaterials would be deposited back in the surrounding medium, usually in the forms of reactive oxygen species (ROS) molecules (T. Guo, 2019).

In the presence of metallic nanoparticles (NPs), interactions with the ionizing radiations will result in Compton effects, X-ray fluorescence, pair production process, photoelectric interactions, or Auger electron emission (Howard et al., 2020). Theoretically, these interactions were influenced by the NPs' atomic numbers (Z) and sizes, as well as the amount of incident radiation energy (Ahmad et al., 2020; Howard et al., 2020). In comparison to the high incident radiation energy, the low energy would

generate a higher mass-energy absorption coefficient between the NPs and the cells or tissues (Ahmad et al., 2020).

The physical differences in ionizing radiation exposure, energy deposition and the energy released would lead to different subsequent chemical and biological effects (McMahon & Prise, 2019). High LET radiations would densely accumulate the energy in the cells and tissues, increasing the ROS production and producing more DNA damages (Howard et al., 2020; McMahon & Prise, 2019). While the NPs are also involved in the physical mechanism, its presence is insufficient to cause damages to the cells, indicating the importance of other possible chemical and biological mechanisms (Howard et al., 2020).

1.2.2 Chemical Phase

Chemical bonds among the atoms and molecules have low energy similar to the quanta of non-ionizing radiation, which could be overpowered by the higher energy of ionizing radiations and promoted the ionization of many molecules of the cells, tissues and medium (Mondelaers & Lahorte, 2001). Byproducts of the ionization is the generation of ROS, which includes both radical and non-radical species. The ROS was generated due to the breakage of the chemical bonds of tissue molecules, especially the water molecules, after the irradiation (IAEA, 2017; Hui Wang, Jiang, Van De Gucht, et al., 2019).

The radical reactions encompass two contrary responses, which are pro-oxidative and scavenging reactions (Cui, 2016; Mondelaers & Lahorte, 2001). Scavenging reactions describe the acts of deactivating the free radicals by some reducing biomolecules agents such as thiol-containing molecules through combinations, disproportionation or electron transfer reactions (Cui, 2016;

Mondelaers & Lahorte, 2001). Meanwhile, pro-oxidative reactions define the encounter of radicals with other biological molecules to produce other radicals by addition or abstraction of radicals, which may lead to further impairments of the cells and tissue components (Cui, 2016; Mondelaers & Lahorte, 2001). The chemical modifiers involved in the responses, such as oxygen would trigger superoxide radicals ($O_2^{\bullet-}$), hydrogen peroxide (H_2O_2) and hydroxyl radicals ($\bullet OH$) (Cui, 2016; P. Ma et al., 2017; “R,” 2017; Zeman et al., 2016).

Both opposite reactions simultaneously occurred during the nanoseconds of post-irradiation, forming a wide range of byproducts. In the end, the robust ionization processes would yield excited molecules, electrons, ions and free radicals in the irradiated system, regardless of the type of the radiation (Mondelaers & Lahorte, 2001). In the presence of matters such as gases, liquids or solids during irradiation, surplus free radicals reactions are stimulated (Mondelaers & Lahorte, 2001). The chemical responses are faster in gases and liquids, compared to the solid matter such as the NPs, which could be detected even months after irradiation (Mondelaers & Lahorte, 2001).

The increment of the effects which were caused by catalysis processes due to the chemical properties of the nanomaterials is termed as the chemical enhancement (T. Guo, 2019). The enhancement is divided into two types including a slight ROS changes and more reaction of interest occurred owing to the catalysis by the surface of the NPs, as well as a high elevation of ROS level with or without the absorption of the radiation by the NPs (T. Guo, 2019). Following the induction of the high amount of ROS, it could initiate the cell apoptosis and cell cycle redistribution (Alan Mitteer et al., 2015; K. Cheng et al., 2018).

1.2.3 Biological Phase

Biological pathways are the most slow-acting processes compared to the physical and chemical phases, involving a complex molecular chain of reactions within both normal and cancer cells at the target sites of RT (McMahon & Prise, 2019). The clinical routine of RT encompasses fractionated irradiations, in which total doses of irradiation were divided and delivered in smaller doses over several weeks (Ray et al., 2015). The gold standard for the RT is that a total of 70 Gy given by 2 Gy over several weeks, and it corresponds to the four Rs principles of radiobiology, as such repair, reoxygenation, redistribution, and repopulation (IAEA, 2017; “R,” 2017; Wray & Lightsey, 2016). Nowadays, there are two additional Rs for the principles of radiobiology, which are radiosensitization and reactivation of antitumor immune responses (Boustani et al., 2019; Cui, 2016; Mayadev et al., 2017). The principles, as illustrated in Figure 1.1, were crucial in understanding the cause and effects of fractionated irradiation dose treatment on the normal and cancer cells. Further literature on the R's of radiobiology would be stated in Section 2.2.

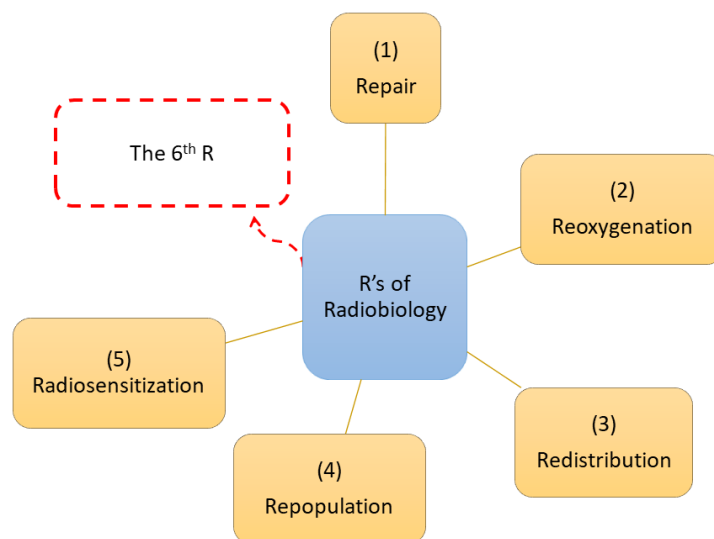


Figure 1.1 The current principles of radiobiology (Boustani et al., 2019; Chew et al., 2021; Cui, 2016; IAEA, 2017; Kesarwani et al., 2018; Mallick et al., 2020; Mayadev et al., 2017; “R,” 2017; Ramroth, 2017; Wray & Lightsey, 2016; Zoipoulou, 2020).

1.3 Nanotechnology and Nanomedicine

Materials in nanometer scales have long existed in our nature. However, only recently that systems and technologies have advanced towards nanoscales application in many fields, including medicine. In medical aspects, many areas have begun to use the nanotechnologies, such as nanogenomics, nanomolecular diagnostics, nanoproteomics, nanopharmaceuticals, nano-arrays, nanofluidics, and NPs (K. K. Jain, 2008). The contributions of nanotechnology in the medical field for prevention, diagnostics, and treatments of diseases were termed as nanomedicine. Nanomedicine hugely plays a role in health sciences, especially in drug delivery, tissue engineering, magnetic resonance imaging, cancer therapy, tissue repair, and cellular therapy (Alarifi et al., 2014; Cui, 2016).

The evolution of nanomedicine started approximately a century ago on the discovery of sugar molecules' size of 1 nm by Einstein, and from then on, there were more inventions for nano-sized molecular analysis and visualization (K. K. Jain, 2008). From the limited resolution of conventional light microscopy, there is scanning X-ray microscopy, which could measure down to 10 nm molecules (K. K. Jain, 2008). Electron microscopy, near-infrared laser microscopy, confocal laser microscopy, fluorescence microscopy, atomic force microscopy and combinations of the microscopy techniques enable the researchers to determine the physical structures of the biomolecules before and after the respective treatments with super imaging resolution and 3-dimensional reconstruction (K. K. Jain, 2008). Nanotechnology was highly beneficial in medical areas as the sizes of the cell biology fundamental features such as the DNA, genome, proteins, and amino acids are in the nanometer scale (K. K. Jain, 2008).

The nanoscale visualization of cellular biology had advanced to integrate nanotechnology into the treatment of diseases by targeting the nanometer biomolecules. For examples, the nanomaterials were utilized in delivering drugs to the targeted sites, promoting regeneration of cells, engineering tissue scaffolds, protecting the healthy sites from free-radicals damages as well as stimulating antibacterial, antiviral and anti-cancer properties (K. K. Jain, 2008; B. Kumar & Smita, 2016). The tissue engineering and tissue regeneration nanotechnology were highly valued in reconstructive surgery treatments (K. Amin et al., 2019; Drouet & Rey, 2020; Mohammadi Nasr et al., 2020; Walsh et al., 2019). Additionally, silver, gold and silica NPs could increase the free radicals production for the toxicity effects towards cancer cells, whereas selenium and cerium oxide NPs could assist the reduction-oxidation (redox) balance by anti-inflammatory and anti-oxidant mechanisms (P. Ghosh et al., 2015; Hirst et al., 2009; Peidang Liu et al., 2019; Misawa & Takahashi, 2011; Passagne et al., 2012). Current chemotherapy research also designated that several types of drugs such as paclitaxel, doxorubicin and cisplatin could be delivered by or co-delivered with metallic-, drug-, or polymeric-based NPs for the better effects (J. Deng, Xun, et al., 2018; X. L. Guo et al., 2019; W. Wang et al., 2015).

NPs are one of the nanobiotechnology classifications (K. K. Jain, 2008). The NPs are defined as an aggregation of matter with a radius of not more than 100 nm (Bhushan, 2010). There are several kinds of NPs that could be synthesized such as inorganic-based (metallic, magnetic, quantum dots), polymeric-based (synthetic, natural, hybrid), and lipid-based NPs (Aliofkhazraei, 2015). Moreover, the various methods of NPs synthesis would yield different shapes of the NPs, for instance, the shape of rods, stars, spheres, triangles, dendrites, ellipsoids, cubes, and cylinders (Aliofkhazraei, 2015; Dasgupta et al., 2014; Gratton et al., 2008; Lee et al., 2019;

Muhammad et al., 2018; Xie et al., 2017). Some of the shapes are depicted in Figure 1.2.

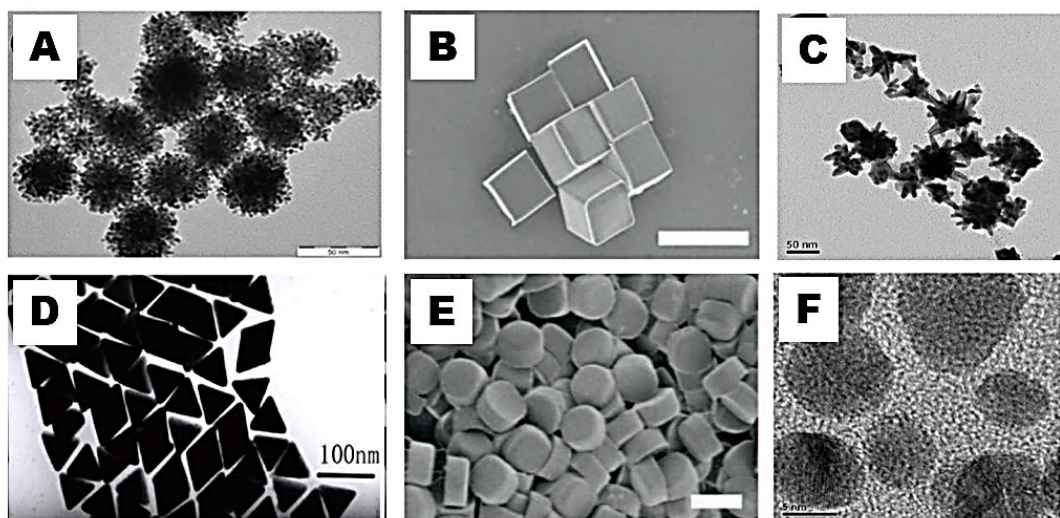


Figure 1.2 Shapes of nanomaterials in the form of (A) dendrites, (B) cubes, (C) stars, (D) triangles, (E) cylinders and (F) spheres. Images are adapted from several published studies (Gratton et al., 2008; Lee et al., 2019; Muhammad et al., 2018; Xie et al., 2017).

The application of therapeutic NPs is the growing trend in the research of RT cancer treatment, in which the NPs with high atomic numbers (Z) are extensively being investigated for their excellent radiosensitization effects. RT is the most common type of curative and palliative treatment for most of cancer patients (IAEA, 2017; Martins et al., 2018). High dose of radiation in eliminating cancer cells usually affected the surrounding healthy tissue and induced several complications (Bingya Liu et al., 2015). The presence of matters called radiosensitizers, such as the NPs, in a tumor would help local absorption of the radiation energy and concentrate more dose at the target site, and thus contributed to the DNA damage of the cancer cells (Wan Nordiana Rahman et al., 2014). Figure 1.3 simplified the mechanism of actions involved in the RT with NPs.

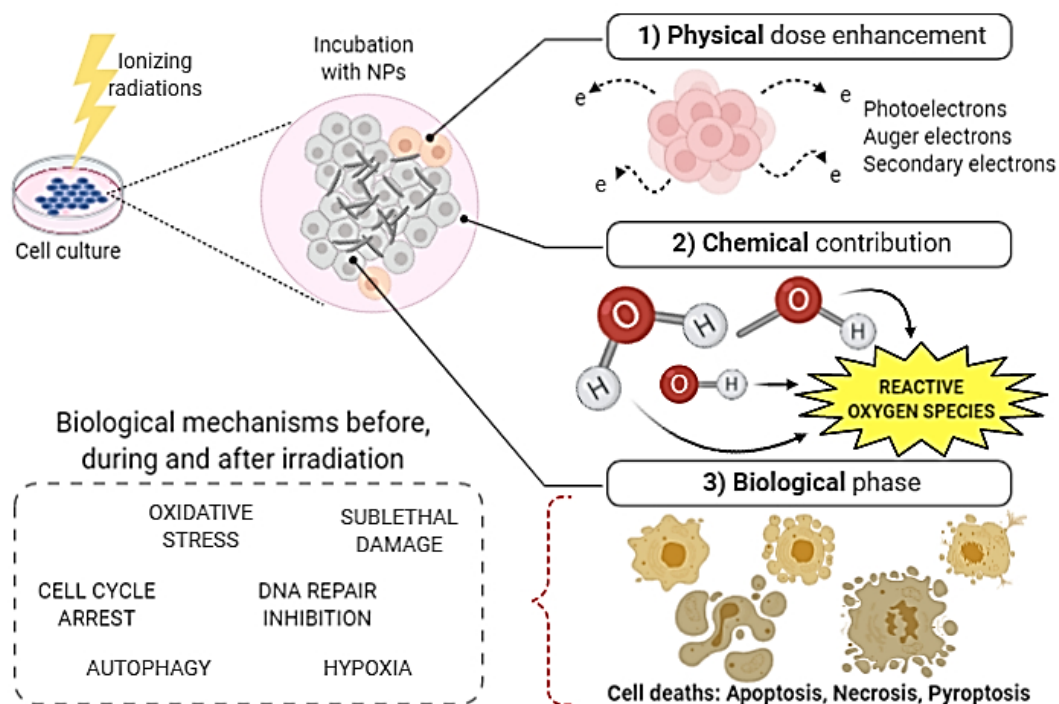


Figure 1.3 Classical radiosensitization process in the presence of therapeutic NPs in RT for cancer treatment. The figure is adapted from Yan Liu et al. (2018).

1.4 Natural Compounds for Anti-Cancer Treatment

Since ancient times, plant extracts are commonly used to treat diseases. In modern days, this type of treatment is known as complementary medicines (WHO, 2013). Complementary medicines are classified as the primary sources of health care in Africa and as the supportive treatment to chemotherapy in European countries and North America (WHO, 2013).

Plants are the principal sources of medicinal phytochemicals that have the potentials to be exploited as a means of cancer therapy (Wahab, 2019). A review reported several types of herbs and natural products used by cancer patients in Middle Eastern countries, such as garlic, honey, turmeric, black cumin, camel milk, stinging nettle, carrot and *Arum palaestinum* (Ben-Arye et al., 2016). Many other pieces of research also validated the anti-cancer and anti-proliferative properties of some plant extracts, for instance, *Ophiocoma erinaceus*, *Sarcopoterium spinosum*, *Clinacanthus*

nutans, *Trigona laeviceps* propolis, *Passiflora foetida* (henna) and *Oroxylum indicum* (*O. indicum*; OI) (Baharara et al., 2016; Buranrat, Noiwet, et al., 2020; Loizzo et al., 2013; Sisina et al., 2017; Umthong et al., 2011; Yong et al., 2013).

The medicinal phytochemicals may induce anti-cancer mechanism and cause the cancer cell death. Apoptosis is one of the anti-cancer mechanisms exerted by the extracts of several plants such as *Dillenia suffruticosa*, *Cordia dichotoma*, *Calophyllum inophyllum* fruit, *Garcinia mangostana* (mangosteen), and OI in pre-clinical cancer cells studies (Foo et al., 2016; D. R. N. Kumar et al., 2012; Moongkarndi et al., 2004; M. A. Rahman & Hussain, 2015; Shanmugapriya et al., 2016; Wahab et al., 2019). Exposure of other extracts from *Kielmeyera coriacea*, *Coriandrum sativum* and OI on several cancer cells had also demonstrated the cell cycle arrest actions (Figueiredo et al., 2014; E. L. H. Tang et al., 2013; Zazali et al., 2013). Other specific anti-proliferative pathways on cancer cells expressed from some other plant extracts included the inhibition of protein tyrosine phosphatase 1B (PTP1B) and serine-threonine kinase (CK2) which have roles in metabolism and cellular proliferation, as well as the disruption of glycogen synthase kinase 3 β (GSK-3 β)-modulated mitochondrial binding of enzyme hexokinase II (Y. Guo et al., 2020; McCarty et al., 2020; To et al., 2020).

As the plant sources have such promising effects for cancer treatments, the plants' compounds could possibly potentiate the actions in RT. More plants are being investigated for their effects in combination with radiations on cancer cells. In HeLa cervical cancer cell line, the extract of *Artemisia kopetdaghensis*, *Kelussia odoratissima* and *Ferula gummosa* had suggested their radiosensitization effects of the 2 Gy dose of γ -radiation from the ^{60}Co units (Fanipakdel et al., 2019; Forouzmand et al., 2018; Hosseini et al., 2017). Corsin, a further purified compound from the saffron

plant, had also demonstrated the high efficacy and radiosensitivity in the head and neck cancer cells (Vazifedan et al., 2017). Natural phenolic compounds, such as curcumin and sinensetin from citrus, were combined with the RT against breast cancer cells and resulted in the enhancement of radiation doses (Minafra et al., 2019; Rezakhani et al., 2020). There were more cancer cell deaths due to the high expression of p53, STAT3 and B-cell lymphoma 2 protein (Bcl2) genes (Minafra et al., 2019; Rezakhani et al., 2020).

1.5 Problem Statement and Rationale of the Study

Chemotherapy has been combined with the RT procedure to boost the treatment performance of certain cancers, and it is termed as chemoradiotherapy (CRT). The chemotherapeutic drugs that are usually served as radiosensitizers are cisplatin, gemcitabine, and doxorubicin (X. L. Guo et al., 2019; Hashemi et al., 2013). Data from clinical studies confirmed the benefits of combined CRT in local tumor control. In comparison to irradiation alone, the results of concurrent CRT were shown to boost the RT effectiveness (A. Mukherjee et al., 2016). A few clinical studies also proved that the effect of the cisplatin in combination with brachytherapy was compelling, and the percentage of disease-free survival after one year was more than 70% (Chandel & Jain, 2016; Hashemi et al., 2013; A. Mukherjee et al., 2016).

The biological rationale is that a chemotherapy drug such as cisplatin could act as a radiosensitizer that can enhance radiation dose at the tumor site. Therefore, treatment could be performed with a lower radiation dose, which will reduce the harmful effects on normal cells. The potential benefit of concurrent CRT is, however, confined by the risk of complication due to the exposure of healthy organs to high dose rate radiation. Cisplatin also induced the formation of toxic platinum intermediates,

which inhibit the post-irradiation DNA damage repairs, which could diminish normal cells' survival (Cui, 2016).

Evidence of survival improvements have been observed, but intrinsic toxicity remains a significant issue with concurrent CRT. There are many side consequences induced by conventional drugs, such as ototoxicity, low blood cell production, menstrual abnormalities, peripheral neuropathy, reproductive problems and the growth of other types of cancer (Chemocare.com, 2016). A study by Aghili and co-workers on combinatorial of cisplatin and medium dose rate brachytherapy indicated the most common side effects were proctitis, leukopenia, cystitis, anemia, vomiting and nausea (Mahdi Aghili et al., 2018).

To widen the therapeutic window of CRT, NPs-based radiosensitizers are introduced. In pre-clinical research, a few metallic elements had shown the potential to be radiosensitizers, such as gold, superparamagnetic iron oxide, platinum, and bismuth NPs (Lazim et al., 2018; Wan Nordiana Rahman et al., 2014; Raizulnasuha Abdul Rashid et al., 2019). Bismuth oxide (Bi_2O_3) NPs (BiONPs) has also been investigated as a potential radiosensitizer (C. Stewart et al., 2016; Taha et al., 2018). The physical justification is that increase in radiation interaction may occur due to the high atomic number of the bismuth element ($Z = 83$), which could instigate more photons absorption and release more electrons even when low radiation energy was being used (C. A. C. Stewart, 2014; Taha et al., 2018; Zulkifli, Razak, Rahman, et al., 2018). In comparison to other types of NPs, the composition of bismuth may trigger additional retention, absorption, and scattering of the radiation at the cancer site, and thus demonstrated a higher enhancement of the dose (Ovsyannikov et al., 2015; C. A. C. Stewart, 2014). A study on radiosensitization of BiONPs, as well as bismuth sulfide, and gold NPs using 3-dimensional (3D) phantom demonstrated that all three NPs could

enhance the kilovoltage radiation with the BiONPs showed the highest effects (Mamdooh Alqathami et al., 2016). GEANT4 was used to simulate brain tissue irradiation in the presence of BiONPs, and the dose enhancement factor (DEF) was quantified up to 18.55, which presented the promising BiONPs capacities (Taha et al., 2018).

Thus, in the present study, BiONPs were selected as the alternative radiosensitizer of cisplatin as well as the combination of both components, which may potentially enhance the radiation dose through the synergetic effects of both compounds. It is anticipated that the radiosensitization effects by combinatorial BiONPs and cisplatin (BC) will be better than the results of combinatorial gold NPs and cisplatin from another study (Cui, 2016).

In regards to their attractive biocompatibility profile, the potential of BiONPs as radiosensitizer has been investigated *in vitro*, *in vivo* as well as *in silico* and phantoms studies which portrayed impressive results (Mamdooh Alqathami et al., 2016; C. A. C. Stewart, 2014; Taha et al., 2018). However, the research above did not investigate the applicability of the BiONPs on breast cancer RT, and this study is the first empirical precedent to apply BiONPs for clinical megavoltage beams.

Due to the toxicity of the commercial synthetic chemo-drugs, researchers started to explore the options for the nontoxic chemotherapeutic agent and radiosensitizers, possibly from natural chemicals and derivatives are of interest (L. Jiang & Iwahashi, 2019). Since the attainment of data on phytochemicals and constituents of medicinal plants in treating and preventing diseases and cancers, especially breast cancers, are significant, it is imperative to discern and identify the active constituents of the plant extracts in order to develop new natural-based drugs or medicine (A. Amin et al., 2009; Buranrat, Konsue, et al., 2020; Foo et al., 2016; Khanna & Mishra, 2019; Safarzadeh

et al., 2014; Shanmugapriya et al., 2016; Sisil et al., 2017; To et al., 2020). *Oroxylum indicum* (OI) leaves extract had been validated to have anti-cancer, anti-virus, anti-oxidant and radiosensitization properties (Wan Nordiana Rahman et al., 2019; Wahab & Mat, 2018). OI leaves are also easily available in Malaysia. The use of plant leaves as the natural-based medicine would also improve the acceptance of the medicine as natural-based agents were expected to have low toxicity *in vitro* and *in vivo* experiments (Awang et al., 2020; Dinda et al., 2015; I. N. Kang et al., 2019; Wan Nordiana Rahman et al., 2019; Wahab & Mat, 2018; Zazali et al., 2013). While OI leaves extract to have the radiosensitizing properties, it is still unknown whether a newly isolated baicalein-rich fraction (BRF) from the same plant gives the same effects due to the different composition of the compounds in the BRF.

Furthermore, most of the previous works on NPs emphasized the dose enhancement by individual NPs as well as a combination with commercial drug only, but the present study applied three components: BiONPs, cisplatin (Cis) and BRF as the prospective radiosensitizers. This study is the first to evaluate the combination of the three components, especially involving the natural compound BRF in combination with the BiONPs (BB) or the BiONPs-Cis (BCB) combination, as well as the RT.

In the cancer treatment, triple drug-based chemotherapy research have been clinically proven in improving the cancer responses compared to a combination of two drugs (Noronha et al., 2015; Somani et al., 2011). However, each drug has its adverse effects, and the act of combining drugs would increase the systemic side effects (Goyal et al., 2016). Recently, Kareliotis et al. (2020) reviewed several modern cancer therapies strategies and concluded that there are the needs of multimodal treatment which required the synergy between the ionizing radiation and sensitizing agents. Thus, this study evaluated the effect of combining BiONPs, Cis and BRF (BCB) to

promote anti-cancer effects while reducing toxicity, as well as to combine natural BRF with BiONPs (BB) to replace Cis in the BiONPs-Cis (BC) combination. This work focused on whether the triple combination of prospective radiosensitizers was more successful than the double combination or single radiosensitizer in stimulating ROS generation, their interactions and cell survival after the clinical RT.

1.6 Objectives of the Study

Investigation of the radiosensitization effects of bismuth oxide nanoparticles (BiONPs) in combination with cisplatin (Cis) and a baicalein-rich fraction (BRF) from *Oroxylum indicum* leaves for clinical radiotherapy beams.

Specific Objectives:

- 1) To determine the cytotoxicity effect of BiONPs, Cis and BRF on MCF-7 and MDA-MB-231 breast cancer cells as well as NIH/3T3 normal fibroblast cells.
- 2) To investigate the reactive oxygen species (ROS) generation and localization of BiONPs within the breast cancer cells and normal fibroblast cells.
- 3) To measure the cell survival and ROS with individual BiONPs, Cis and BRF and combinatorial BiONPs-Cis (BC), BiONPs-BRF (BB) and BiONPs-Cis-BRF (BCB) using clinical RT beams (^{192}Ir of γ -rays, 6 MV of photon and 6 MeV of electron beams).
- 4) To radiobiologically evaluate the type of interactions (synergism, additive effects or anatagonism) for the radiosensitization effects of 3 individual treatments (BiONPs, Cis and BRF) as well as 3 combination treatments (BC, BB and BCB combinations) for their potential applications in clinical CRT.

- 5) To analyze the involvement of apoptosis mechanism after treatment exposure, with the selected treatment components.
- 6) To identify the subcellular biochemical and structural changes using Raman spectroscopy after treatment exposure with the selected treatment components.

1.7 Thesis Outline

There are six chapters in this thesis.

Chapter 1 is an introduction to the RT, radiosensitization mechanism, nanotechnology nanomedicine, as well as natural anti-cancer agents. The problem statements and objectives of the study are also explained.

Chapter 2 articulates the overview of the breast cancers data as one of the focus in this study. The application of several kinds of radiosensitizer in RT, such as metallic nanoparticles, anti-cancer drugs and natural compounds, were included in this chapter. Detailed types of molecular characterization methods of the radiosensitization effects were also mentioned.

Chapter 3 contains specific protocols in preparing the treatment components, culturing the cell lines, testing the cytotoxicities of the treatment components, measuring the ROS generation, and setting up the irradiation of ^{192}Ir of γ -rays, photon and electron beams. This chapter also explained the post-irradiation assay and analysis, such as clonogenic assay as well as the analysis of cell survival, combination treatment interactions, ROS generation, apoptosis using MuseTM flow cytometry, and subcellular changes by Raman spectroscopy.

Chapter 4 reported the results of the experiments in the study. Based on the results of the cytotoxicity of the BiONPs, Cis and BRF, the safe concentrations were chosen for the subsequent experiments of irradiations. The SER were extrapolated

from the survival curves and compared to the theoretical dose enhancement factor (DEF). One of the best combination treatments were selected for the following apoptosis and subcellular changes analysis. The results also involved statistical results.

Chapter 5 explains the findings in the previous chapter, which were supported by other previous studies.

Chapter 6 summarizes the findings and conclusion in a few sentences for each part of the study.

1.8 Research Scopes

This thesis is divided into 3 phases of study.

Phase 1: The biocompatibility study of BiONPs, Cis and BRF.

Phase 2: The radiosensitization studies of BiONPs, Cis, BRF, BC, BB, and BCB treatments.

Phase 3: The mechanism of action studies of the selected radiosensitizer combination.

The first phase is the part of biocompatibility studies of three types of prospective radiosensitizers, which are metallic nanoparticles (BiONPs), commercial chemo-drug (Cis), and natural compound from OI plant leaves (BRF). The cytotoxicity, cellular uptake, and reactive oxygen species (ROS) generation induced by BiONPs were initially investigated 3 cell lines, which were 2 different subtypes of breast cancer cell lines (MCF-7 cells and MDA-MB-231 cells) and 1 normal cell line (NIH/3T3 cells). The ROS generation by the BiONPs incubation with the cells were found to be incoherent with the cytotoxicity results. At the end of this stage, the one

safe concentration of each individual treatment component was determined as 0.5 mM of 60 nm of BiONPs, 1.30 μ M of Cis and 0.76 μ g/ml of BRF.

Second phase is the radiosensitization studies of BiONPs, Cis, BRF, BC, BB, and BCB treatment components. Quantification of radiosensitization effects and ROS generation were conducted for ^{192}Ir of γ -rays, 6 MV of photon beam, and 6 MeV of electron beam. The synergetic interactions of the combination treatment and linked to the SER values. The experimental SER values were also compared to the calculated theoretical DEF values for the monoenergetic beams of ^{192}Ir of γ -rays and 6 MV of photon beam. The ROS generation after the treatment exposure were deduced to be insignificant and could not predict the survival fractions of the cells. Finally, the components that were established to cause the optimum synergetic radiosensitization effects are BC combination for the ^{192}Ir of γ -rays on MCF-7 breast cancer cells.

The last part is the mechanism of action studies of the chosen radiosensitizer combinations. Apoptosis analysis for 14 and 40 hours after the exposure of MCF-7 breast cancer cells to the BC combination and the 0, 2 and 4 Gy of ^{192}Ir of γ -rays to enlighten the cells death mechanism. Meanwhile, Raman spectroscopic analysis were conducted to elucidate the subcellular biochemical changes after the exposure of MCF-7 breast cancer cells to the BC combination and the 0, 0.5 and 2 Gy of ^{192}Ir of γ -rays. Radiosensitization processes were discovered to occur predominantly due to early apoptosis, as well as the involvement of glycogen increment, amino acid disarrangement and DNA/RNA disturbance.

CHAPTER 2

LITERATURE REVIEW

This chapter presents the reviews on breast cancers, the potential of several types of radiosensitizers, such as NPs, drugs and natural compounds, as well as the intricate mechanisms which may transpire to result in the radiosensitization effects.

2.1 Overview on Breast Cancers

Globally, breast cancers had accounted for up to 2 million new cancer cases in 2018, nearly similar to the number of lung cancers followed by colorectal, prostate and stomach cancers (IARC, 2014; WHO, 2019a). The breast cancer is the leading cause of death for women in 103 countries (WHO, 2019a). The incidence frequency was the highest in Northern and Western Europe, as well as New Zealand and Australia (Bray et al., 2018).

In Malaysia, there were approximately 43 thousand number of new cancer cases in 2018, and the breast cancers accounted for up to 7.5 thousand cases of it (WHO, 2019b). 32% of the females' cases were also attributable to the breast cancers, followed by colorectal cases (12%), cervical cancer (7%), and ovarian cancer (5%) (WHO, 2019b). While breast cancer ranked the first as the most frequent new cancer cases in Malaysia, it was ranked second for the number of total cancer death which come after lung cancer-induced deaths (WHO, 2019b).

According to the Malaysia National Cancer Registry Report (MNCR), a higher number of breast cancer cases were detected in 2012 to 2016, compared to the previous 5-years period (Azizah et al., 2020). For the year 2012 to 2016, breast cancers were commonly diagnosed in Chinese ethnic with 40.7%, followed by Indians (38.1%) and

Malays (31.5%) (Azizah et al., 2020). Comparatively, Malaysian Chinese breast cancer incidence rates were lower than the rates from Singaporean Chinese, as well as patients from Maori (New Zealand), New South Wales (Australia), Osaka (Japan), Seoul (Korea), and Cali (Columbia) (Azizah et al., 2020). Nonetheless, breast cancers were the most commonly detected in Malaysian females group regardless the ethnicity, with the percentage of 34.6 to 36.8%, and the highest incidence rate was in the 60-64 age group (Azizah et al., 2020).

The report also specified that early screening of the female breast cancers in the year of 2007 to 2016 detected the highest incidence rate of stage 2 breast cancers, followed by stage 3, stage 4 and stage 1 (Azizah et al., 2020). According to a breast cancer research organization, cancer stages could be categorized according to sizes (as illustrated in Figure 2.1), effects on the lymph nodes, and the metastasis sites (Breast Cancer Now Ltd., 2018).

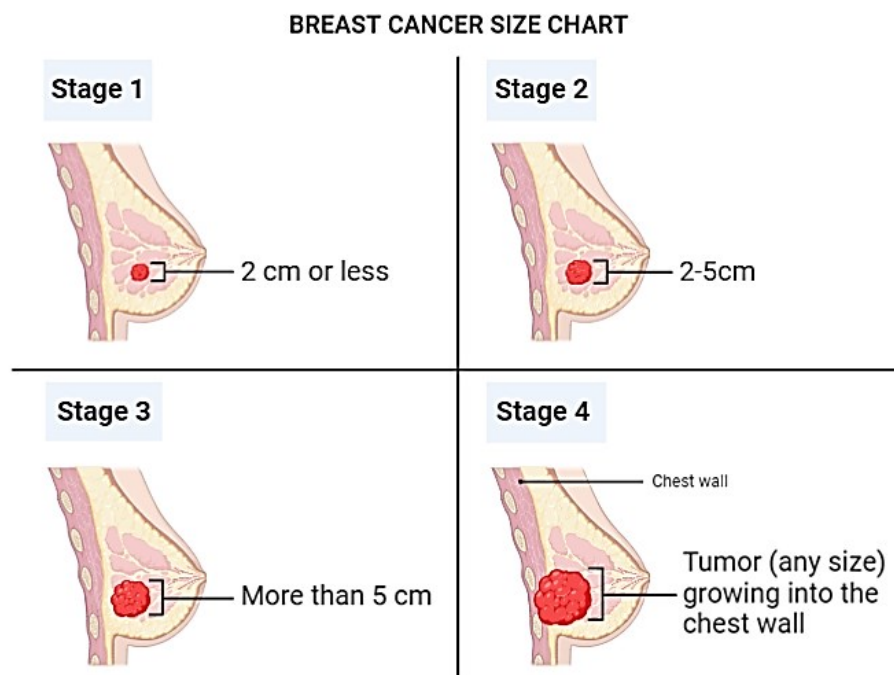


Figure 2.1 Stages of breast cancers according to the tumor sizes. Illustration was adapted from Breast Cancer Now Ltd. (2018)

In the male group, 291 cases were identified from 2012 to 2016, which apportioned to 135 cases were from the Malay race, 125 cases were from the Chinese race, and 21 cases were from the Indian race. (Azizah et al., 2020). The summary also listed Selangor as the state with the top detection of breast cancers, and Wilayah Persekutuan with the least number of detection (Azizah et al., 2020).

Furthermore, there are many subtypes of breast cancers clinically, which could be classified into several categories, as in Table 2:1

Table 2:1 Clinical categories of breast cancers

Categories	Subtypes	References
Pathology/ histological	1) Invasive ductal carcinoma 2) Invasive lobular carcinoma 3) Ductal carcinoma in situ (DCIS) 4) Other (includes tubular carcinoma, medullary carcinoma, mucinous carcinoma and mixed carcinoma)	Banerji et al. (2012); Pandit et al. (2020)
Histological malignancy	1) Benign: Adenosis, fibroadenoma, phyllodes-tumor, and tubular-adenoma 2) Malignant: Ductal, lobular, mucinous, and papillary	Jannesari et al. (2019)
Molecular/ hormonal/ receptor	1) Hormone Receptor Sensitive (HRS), which involved estrogen receptor (ER), progesterone receptor (PR), and human epidermal growth factor receptor 2 (HER2): a. Luminal A (ER+ and/or PR+/HER2–), b. Luminal B (ER+ and/or PR+/HER2+), 2) HER2-enriched (ER– and PR–/HER2+), or c-erb2 gene overexpression 3) Triple-negative (ER– and PR–/HER2–), or basal-like breast cancer 4) Normal-like 5) Unknown	Banerji et al. (2012); Ganggayah et al. (2019); Pandit et al. (2020)

Correspondingly, preclinical experimental works also involved breast cancer cell lines, which originated from humans and animals, with the most used subtypes are MCF-7

and MDA-MB-231 human breast cancer cells. Other subtypes of breast cancer cells that were scarcely utilized in research are listed in

Table 2:2.

Table 2:2 Types of breast cancers lines used in pre-clinical studies.

Cell lines	Origin	Reference
4T1	Mouse origin and mimics the stage 4 of human breast cancer cells	DuRoss et al. (2019); J. Liu et al. (2019)
MDA-MB-361	Human origin and metastasizes at brain	Dinkelborg et al. (2019); Shpyleva et al. (2011)
MDA-MB-468	Human origin	Altemus et al. (2019); Dinkelborg et al. (2019); Peng Liu et al. (2016)
T47D	Ductal carcinoma	Dinkelborg et al. (2019); Rollando and Prilianti (2018); Shpyleva et al. (2011)
SK-BR-3	Caucasian ethnic	Jaeger et al. (2017); Jafarzadeh et al. (2018); Peng Liu et al. (2016)
BT-474	Ductal carcinoma	Jaeger et al. (2017); Peng Liu et al. (2016)
BT-549	Ductal carcinoma	Altemus et al. (2019); Dinkelborg et al. (2019); Shpyleva et al., (2011)

Clinically, different cancer cell subtypes would require different treatment approaches, specifying the more targeted treatments (IARC, 2014). Generally, the primary treatment for breast cancers is chemotherapy, hormone therapy and surgery (Ganggayah et al., 2019). Among the breast cancer patients at all hospitals in Kelantan (years of 2007 to 2011) and University Malaya Medical Centre (years of 1993 to 2016), the data recorded that only 19.1% and 49.4% of the patients, respectively, were